A multimodal Mass Spectrometry Imaging approach for the study of musculoskeletal tissues

Sanaullah Chughtai[1], Kamila Chughtai[1], Berta Cillero Pastor[1], András Kiss[1,3], Prashant Agrawal[2,§], Luke MacAleese[1,*], Ron M.A. Heeren[1,3]

[1]FOM-Institute AMOLF, Science Park 104, 1098 XG Amsterdam The Netherlands

[2] Eindhoven University of Technology, Den Dolech 2, 5612 AZ Eindhoven, The Netherlands

[3]The Netherlands Proteomics Centre, H.R. Kruytgebouw, East 6.11 Padualaan 8, 3584 CH Utrecht, The Netherlands

[§] Current Address: Ira Agrotech and Research Pvt Ltd, B 1/2, MIDC, Butibori, Nagpur, (MS) India - 440015

[*] Current Address: Université Claude Bernard Lyon 1, 43 boulevard du 11 Novembre 1918, 69622 Villeurbanne cedex, France

Email addresses:

Sanaullah Chughtai: chughtai@amolf.nl

Kamila Chughtai: czornak@amolf.nl

Berta Cillero Pastor: cillero@amolf.nl

András Kiss: kiss@amolf.nl

Prashant Agrawal: aprashantr@gmail.com

Luke MacAleese: luke.macaleese@lasim.univ-lyon1.fr

Corresponding author

Ron M.A. Heeren: r.heeren@amolf.nl Tel. +31-20-7547100 Fax. +31-20-7547290

Abstract

Imaging mass spectrometry combines the chemical sensitivity and specificity of mass spectrometry with microscopic imaging resolution. The ability to simultaneously obtain images from analytes detected allows us to know the composition of the surface of a thin tissue section. Although the technology is very well known and different applications have been used like in the classification of different diseases, little has been done in musculoskeletal tissues. Rheumatoid Arthritis (RA) is a widespread musculoskeletal disease that exhibits an extensive molecular complexity that is poorly understood. In this paper a multimodal mass spectrometry imaging (MSI) strategy was applied to identify and localize biomolecules such as lipids, peptides and proteins in bone, muscle or skin from the limb of a mouse model of RA. High spatial resolution Secondary Ion Mass Spectrometry (SIMS) was used to image the elemental and small molecular distributions. Matrix Assisted Laser Desorption/Ionization (MALDI) molecular imaging complemented these studies revealing a specific distribution of phospholipids and peptides/proteins. A profiling protocol that employs “on tissue digestion/off tissue analysis” was successfully established for orthogonal peptide/protein identification. Among the identified proteins were cytokines (like interleukin 18), cytoskeleton related proteins (actin, tubulin or myosin) or proteins of the family of metalloproteinases (AST2) that are involved in inflammation triggering and autoimmune responses in RA. The results of this multimodal MSI and complementary proteomics approach resulted in a multitude of protein localizations and local interactions that reveal detailed molecular signatures from the different regions that constitute the musculoskeletal tissues affected by RA. The information provided by multimodal SIMS and MALDI imaging, reveals new and future possibilities for the study of musculoskeletal diseases.

Keywords:
Mass Spectrometry Imaging
Rheumatoid Arthritis
Proteomics
MALDI
SIMS

1. Introduction

Mass spectrometry imaging (MSI) is becoming a widely used discovery tool used for *ex vivo* visualization of molecules such as drugs, lipids, peptides and proteins directly from a variety of thin tissue sections [1]. MSI allows the rapid detection, localization and identification of many molecules from the most complex, biological sample surfaces. It is a label free technique that can deliver detailed spatial information of molecules of interest on different length scales, from subcellular to multi-cellular level and from organs to whole biological systems.

MSI has been applied to a vast spectrum of pathologies such as neurodegenerative (Parkinson's disease and Alzheimer's disease) [2, 3], metabolic (Fabry's disease and nonalcoholic fatty liver disease) [4, 5], muscle [6] and kidney [7] diseases. Similarly, many cancer types such as breast cancer [8], prostate cancer [9], ovarian cancer [10], lung cancer [11] colon cancer and liver metastasis [12] were investigated using MSI. The majority of the previously published works have been performed in soft tissues like brain, kidney, lung, heart or liver. However, little has been published about how useful MSI technology can be in the study of heterogeneous, hard and complex tissues like musculoskeletal tissues. Among the different pathologies that affect these complex tissues we find Rheumatoid Arthritis (RA). RA is an autoimmune disease that causes chronic inflammation of the joints and muscles, bone destruction and affects many other organs of the body. For that reason is often referred to as a systemic illness. Uncontrolled active RA causes joint damage, disability, decreased quality of life, as well as cardiovascular and other co-morbidities [13]. The exact cause or trigger of RA is largely unknown. Although a number of factors such as infectious agents (viruses, bacteria, and fungi), environmental factors (smoking) and genetic predisposition have long been suspected, none has been proven to be a direct cause [13]. Mass spectrometry (MS) has historically played an important role in the identification of new proteins from sera of patients with different musculoskeletal disorders. Gas chromatography-mass spectrometry (GC-MS) and high-performance liquid chromatography (HPLC)–electrospray ionization-mass spectrometry (ESI-MS) have been used to phenotype serum samples of RA patients [14]. The versatile nature and high sensitivity of MS proved to be useful in disease biomarker identification [15]. Protein differential display techniques such as two-dimensional gel electrophoresis (2-DE) combined with MS, one-dimensional or two-dimensional liquid chromatography MS (LC-MS), has

become increasingly useful to establish differential protein profiles [16]. These techniques couple to MALDI-TOF-MS analysis have been performed to observe the differential proteome expression in the plasma and synovial fluid of RA, osteoarthritis (OA) and reactive arthritis patients [17]. The investigation of RA synovial fluid [17-21], synovial fibroblasts [22-24], blood plasma [17, 25, 26], blood serum [16, 27, 28] and human whole saliva [29] led to the discovery of a number of potential biomarkers such as actin [25, 30, 31], inflammatory cytokines and proteins related to lipid metabolism [16, 18, 21, 32]. Although recent years witnessed the progress in a number of studies exploring the etiology and pathogenesis of RA, its molecular pathological mechanism is still largely unknown and open to further investigations [16]. The diagnosis and choice of the appropriate therapy for patients remains very challenging.

Animal models of autoimmune arthritis have proven to be valuable research tools for the study of pathogenic mechanisms of rheumatic diseases as well as for testing new therapies. Several mouse models of arthritis have been established, including those that require immunization with antigen: proteoglycan induced arthritis, streptococcal cell-wall arthritis or collagen induced arthritis (CIA). CIA has been the most widely studied model of RA. It shares several pathological features with RA, and Collagen II is a major protein in cartilage [33]. The CIA model has been used extensively to identify potential pathogenic mechanisms of autoimmunity, including the role of individual cell types in disease onset and progression, as well as to design and test new therapeutics. The CIA model has been also used to test new biologically based therapeutics [34, 35].

As we have explained above, classical MS techniques provide detailed insight into the composition of a sample, however very few studies target the investigation of the local etiology and pathogenesis in the area where the disease is actively occurring. Although immunohistochemistry and conventional staining techniques can study selected proteins in histological sections, they do not provide the wealth of information obtained by high performance MS studies on body fluids. One way to overcome this limitation of classical histology is to perform MS profiling and Mass Spectrometric Imaging (MSI) directly on a tissue section, an approach often referred to as molecular histology. Here, we present for the first time, the application of MSI and MS profiling for identification and localization of biomolecules in musculoskeletal tissues directly from a RA mouse model.

2. Materials and Methods

2.1 Chemicals

The MALDI matrix α-cyano-4-hydroxycinnamic acid (CHCA) and the modified proteomics grade trypsin were purchased from Sigma (Schnelldorf, Germany). Ethanol, HPLC grade water, acetonitrile (ACN) and trifluoroacetic acid (TFA) were purchased from Biosolve (The Netherlands). Gelatin was purchased from Fluka (Germany). Dithiothreitol (DTT) and iodoacetamide were purchased from Sigma (Germany). All compounds were used without further purification.

2.2 Experimental Workflow

The experimental workflow employed in the entire study is shown in **figure 1**. It describes the sequence of sample preparation, profiling and imaging experiments from the RA samples collected. After tissue sectioning the samples were washed, digested and sprayed with matrix preventing the de-localization of molecules and analyzed to visualize peptides by MALDI-MSI. MALDI-MSI performed on unwashed, matrix coated tissue sections, helped to localize various lipids. SIMS imaging required only a gold coating and immediately provided high spatial resolution images of RA tissue sections. These high resolution images were particularly useful to study small joint areas that are more difficult to observe with the lower spatial resolution obtained in the MALDI-MSI experiments. Complementary protein profiling on tryptically digested tissue homogenates with MALDI MS/MS was performed and resulted in a small protein database. This database was later used to validate the interpretation of the on-tissue digested MSI results.

2.3 Sample preparation

The RA mouse model was obtained from Eindhoven University of Technology, The Netherlands. All handling and use of animals complied with Dutch animal welfare legislation, including the animal housing and termination that in addition was approved by the University Animal Welfare Officer. DBA/1 male mice (age 10 weeks) had Collagen Induced Arthritis (CIA) using heterogeneous type II collagen. Development of RA in the treated animals was monitored by a physical examination of inflamed joints and MRI scanning (data not shown). One mouse was sacrificed 24

hours after the development of RA symptoms. Mouse limbs were dissected and embedded into gelatin and immediately frozen by gently lowering the embedded tissue into liquid nitrogen for 60 seconds. Samples were then stored at -80 °C until further analysis. Gelatin embedded limbs were sectioned into 12-µm thin sections using a cryo-microtome (HM525, MICROM, Germany) and thaw-mounted onto 25x50x1.1 mm Indium Tin Oxide (ITO) coated slides (Delta Technologies, USA) with a specific surface resistance of 4-8 Ω. Slides were stored at -80 °C until further analysis. All the experiments were performed in the right and left inferior limbs and in three independent samples of each of them.

2.4 SIMS-MSI of small molecules

Prior to SIMS analysis the slides were defrosted and dried in a vacuum desiccator at room temperature (RT) for 30 minutes, followed by gold-coating using a Quorum Technologies (New Haven, UK) SC7640 sputter coater equipped with a FT7607 quartz crystal microbalance stage and a FT690 film thickness monitor to deposit 1 nm of gold layer. Data was acquired using a Physical Electronics TRIFT II (Physical Electronics, USA) time of flight secondary ion mass spectrometer (SIMS-TOF) equipped with an Au liquid metal ion gun tuned for 22 keV Au^+ primary ions. Images were acquired with a mosaic of 256x256 pixel rasters that each measures a dimension of 187.5x187.5 µm. As a result each pixel in the SIMS raw data set is substantially smaller than 1 micrometer. Data was analyzed and visualized using WinCadence software version 4.4.0.17 (Physical Electronics, USA).

2.5 MALDI-MSI of lipids

Slides were dried in a vacuum desiccator at RT for 30 minutes. A 10 mg/ml solution of CHCA in 1:1 ACN:H_2O/0.1% TFA was applied on the surface of the tissue slides using a vibrational sprayer (ImagePrep, Bruker, Germany). Samples were analyzed on MALDI-HDMS system (Synapt, Waters, UK) in positive ion mode utilizing both the time of flight and ion mobility separation (IMS) modes. The images were acquired with a laser spot size of 100-µm using a microprobe mapping grid with spots spaced in an array of 150x150-µm. Total ion current (TIC) normalization was used for data analysis and visualized with BioMap software (Novartis, Switzerland). data was processed using MassLynx, Driftscope and HDI software (Waters, UK).

Lipids were identified by comparing the masses to known lipid standards or by SimLipid software v2.1 (PREMIER Biosoft International, USA).

2.6 MALDI-MSI of peptides/proteins

Tissue sections were immersion washed in a Petri dish. The procedure involved two subsequent washes in 70% ethanol for 30 seconds, followed by a single 90% ethanol wash for 30 second. After washing, slides were dried in a vacuum desiccator for 30 minutes. Trypsin was resuspended in water at a concentration of 0.05 µg/µL. Droplets of 20 nL of this trypsin solution were deposited on the tissue surface in a 150x150-µm raster by CHIP 1000 chemical inkjet printer (Shimadzu, Japan). During trypsin application, the target stage was kept at 37 ºC. Tissue sections were incubated in a humidified chamber at 37 ºC for 12 hours. Matrix application and imaging were performed as described in section 2.4 after completion of the digestion.

2.7 MALDI-MS profiling of peptides/proteins in solution digestion

1.5 mg of tissue sections of three independent samples were intermittently collected during the sectioning process. These tissue sections were homogenized by sonication for 5 minutes to facilitate protein screening with MALDI-MS. The homogenates were centrifuged and filtered to remove cell debris. The supernatant containing the proteins was reduced by adding 5 µl of 200 mM DTT solution in 100 µl sample for 45 min at room temperature and alkylated by adding 4 µl of 100 mM iodoacetamide solution in the reduced sample for 45 min at room temperature. The excessive iodoacetamide was neutralized to stop the alkylation process by adding 20 µl of 200 mM DTT in the sample solution followed by incubation for 45 min at room temperature. The reduced and alkylated sample was digested in solution by adding trypsin, followed by incubation at 37 ºC for 12 hours. The resulting tryptic peptide solution was mixed with the CHCA matrix solution (10 mg/mL) in 1:1 ratio v/v and 1 µL of this mixture was spotted on a MALDI target plate. Data dependent analysis (DDA) of tryptic peptides was performed with a combination of MS and MS/MS scans in MALDI-Q-TOF instrument (Synapt, Waters, UK) using a MALDI survey method. Briefly, data directed acquisition by the MALDI survey method was fully automated with a predefined target plate motion pattern and time specified for switching from MS survey scan to MS/MS, and from one MS/MS to another. Within each well, as many

parent ions meeting the predefined criteria (all peaks within the *m/z* 100-3000 range, divided into 50 *m/z* range windows) will be selected for CID MS/MS using argon as collision gas and a mass dependent collision energy until end of probe pattern was reached, starting from the most intense peak. The LM and HM resolution of the quadrupole (15.3 and 15.0 respectively) were both set to give a precursor selection window of 2 Da. The instrument was externally calibrated to less than 2 ppm accuracy over the mass range of *m/z* 100 - 3000 using sodium iodide and PEG 200, 400, 600, 1000, 2000 and 3500 mixtures. Individual spectra from each of the MS survey and MS/MS performed were combined, smoothed, deisotoped and centroided using the MassLynx (Waters, UK) software. The combined MS/MS peptide ion data were sent to Mascot algorithm as peaklist (.pkl) files using the Swissprot database (*Mus musculus* 2011 database) to identify the proteins. The parent and fragment ion tolerance were set to 1.2 Da. The search criteria included up to two missed cleavages, oxidation of methionine and proline as variable modifications and CarbamidomethylDTT (C) as a fixed modification. The amino acid sequence tag obtained from each peptide fragment was used for protein identity. Identifications were considered positive based on a score calculated by Mascot algorithm (Matrix Science version 2.3.02) with a threshold of $p<0.05$.

2.8 MALDI-MS profiling of peptides/proteins by on tissue digestion/off tissue analysis

In this approach trypsin solution was applied directly on tissue sections by pipette and incubated for 6 hours in a humid chamber kept at 37 ºC. After incubation, the solution containing the tryptic peptides was collected by pipetting the droplet of the tissue. Subsequently it was mixed with CHCA matrix solution (10 mg/mL) in 1:1 ratio v/ 1 µL of this mixture was spotted on a MALDI target plate. Data dependent analysis (DDA) of tryptic peptides was performed by MALDI survey method described in section 2.7.

2.9 Histological staining

Hematoxylin and eosin (H&E) staining was performed on tissue sections adjacent to the sections that were subjected to MSI. The stained slides were scanned using a MIRAX (Carl Zeiss, Germany). The histological images were aligned with the MALDI ion images using BioMap software (Novartis, Switzerland).

3. Results

Multimodal MSI in combination with histological staining was employed to study various classes of biomolecules present in the RA mouse model. High spatial resolution SIMS imaging revealed the distribution of small molecules and lipids, while MALDI-TOF analysis was performed to localize lipids and peptides. The anatomical features observed in the adjacent histological stained sections were employed to co-register the different imaging modalities. The **supplementary figure 1** shows typical results from four different imaging modalities, optical blockface imaging (**A**), H&E histological staining (**B**), SIMS-MSI (**C**) and MALDI-MSI (**D**), which were used throughout this study. All imaging modalities provide specific and complementary morphological and molecular information at a different spatial resolution. The **supplementary figure 1A** shows the different parts of a mouse leg: knee joint (I), muscle (II), the fibula and the tibia (III), the ligaments (IV) and the femur underneath the muscle (V). In **supplementary figure 1B** the H&E staining allows us also to visualize these tissues. **Supplementary figures 1C** and **1D** are examples of images acquired by SIMS or MALDI-MSI respectively.

3.1 MSI of lipids and elements in musculoskeletal tissues in a RA mouse model

3.1.1 TOF-SIMS

The elemental traces like sodium, potassium and calcium as well as lipids are the abundant species present in the spectra from biological tissues. We have performed high resolution TOF-SIMS experiments on 12-µm thick gold-coated sections to identify and localize these elements. The distributions of different molecules such as sodium (Na) *m/z* 23, potassium (K) *m/z* 39, calcium (Ca) *m/z* 40, and lipids of different masses were clearly marked from the distinct regions as **figure 2** shows. In **figure 2A** the total ion image is represented. In **figure 2B** the signal from potassium is represented in red color observing a high intensity in the muscles. The signal from sodium is represented in green color observing a high presence in the femur. Some areas of the skin present an orange color due to the overlapping of the potassium (red) and sodium signal (green). The area of the joint has a lower signal compared to the muscle or skin. An Indium ion image (*m/z* 115) from the glass slide was used as a background to add contrast to the images of ions of interest. In **figure**

2C the *m/z* 184 from phosphocoline (PC) head group is represented in red color observing a homogeneous distribution in the entire sample, even in the core of the joint. However the *m/z* 791 from PC 36:0 (represented in green color) is more prevalent in the area of the muscles. Diacylglycerol (DAG) (*m/z* 577) is represented in blue color observing its presence in the skin but also in the joint. An accumulation of DAG can be appreciated in the upper part of the limb. In **figure 2D** cholesterol (*m/z* 369), represented in red color, is observed in the muscles but with a higher intensity in the femur. As we explained earlier, potassium is present basically in the muscles, here represented as green color. In **figure 2E** cholesterol (*m/z* 369), represented in red, is very abundant in the muscles and in the femur. The *m/z* 577 DAG accumulations are more evident in this figure (represented in green). **Figure 2F** shows the co-localization of cholesterol (in red) and calcium *m/z* 40 (in green) in the muscles. However, calcium spots have the highest signal and they are observed in the femur.

3.1.2 MALDI-MSI

As we already observed with SIMS, a lipid investigation was also undertaken by MALDI imaging of the 12-µm thick tissue sections (**Figure 3**). The distribution of PC related molecular ions such as (**A**) PC 32:0(16:0/16:0) $[M+H]^+$ at *m/z* 734.5; (**D**) PC 36:1(18:0/18:1) $[M+H]^+$ at *m/z* 788.5 and (**F**) PC 40:6(18:0/22:6) $[M+H]^+$ at *m/z* 834.5 were abundant in the lower part of the limb including the joint and the muscles. The distribution of lipid molecular ions such as (**B**) PC 34:2(16:0/18:2) $[M+H]^+$ at *m/z* 758.5 and (**E**) PC 34:2(16:0/18:2) $[M+K]^+$ at *m/z* 796.5; were specific from the upper limb. Other species like (**C**) PC 34:1(16:0/18:1) $[M+H]^+$ at *m/z* 760.5 were more homogeneously distributed.

3.2 MALDI-MSI of peptides in musculoskeletal tissues in a RA mouse model

MALDI-MSI trypsin digested tissue sections revealed the spatial localization of various tryptic peptides on the tissue surface. Their identity was subsequently confirmed on-tissue MS/MS profiling experiments on regions with sufficient peak intensity. Additional confirmation was obtained by the exploration of the small database generated from the tissue homogenate MALDI profiling experiments. The distributions of various high abundant peptides are presented in **Figure 4A-I**. The actin tryptic peptide at *m/z* 1198.7 (**A**) and myosin tryptic peptide at *m/z* 1885.7 (**B**)

were abundant in the muscles. Tubulin (TBCC) tryptic peptide at *m/z* 1960.0 (**C**), troponin T (TNNT3) tryptic peptide at *m/z* 1887.9 (**D**), collagen alpha-1(XIX) chain (COJA1) at *m/z* 1584.8 (**E**), collagen alpha-2(I) chain (CO1A2) at *m/z* 1561.8 and (**F**) tyrosine-protein phosphatase non-receptor type 12 (PTN12) at *m/z* 1654.8 (**G**), were also found in the muscles but with a higher concentration in the lower part of the limb. Peptides from the leukocyte receptor cluster member 8 homolog (LENG8) at *m/z* 1027.8 (**H**) and EF-hand calcium-binding domain-containing protein 5 (EFCB5) at *m/z* 1197.7 **(I**) had a completely different localization. Both peptides were highly distributed in the skin and in the ligaments from the lower limb.

We have also plotted the distribution of RA related peptides from proteins like disintegrin and metalloproteinase with thrombospondin motifs 16 (ATS16) at *m/z* 1347.7 (**figure 5A**), pro-interleukin-16 (IL-16) at *m/z* 1404.7 (**figure 5B**) highly distributed in muscles, bones and ligaments. Disintegrin and metalloproteinase with thrombospondin motifs 2 (ATS2) at *m/z* 1838.9 (**figure 5C**) was also detected in those areas but with a lower signal.

3.3 MSI and ion mobility separation capabilities

MALDI imaging of heterogeneous tissue types, such as found in this RA model, requires additional separation capabilities to make a distinction between the various molecular classes of molecular ions obtained from tissue sections. Ion mobility based gas-phase separation of MALDI generated ions is a new strategy to tackle this issue [36]. **Figure 6A** represents a spectrum of detected ions in the mass range *m/z* 650-950 on ion mobility mode and detected directly from the tissue sections. The plot of the drift time versus *m/z* shows how many ions with the same *m/z* value have a different drift time (**figure 6B**). Thus, selecting a specific mass range we can separate the signal from the background ion at *m/z* 721.41 (**figure 6C**) from the mass at *m/z* 721.49 specific from the upper part of the limb (**figure 6D**). In this way we show how ion mobility helps to separate less intense ions.

3.4 Proteome pathway analysis

Protein profiling experiments were performed directly on the mouse tissue sections as well as on tissue homogenates. Data dependent analysis (DDA) was used in both cases to identify proteins from these tissues and known RA markers. A profiling approach employing on-tissue digestion followed by off-tissue analysis was

used in order to increase the number of identified proteins. This approach provided minimum tissue processing and allowed the usage of similar analytical conditions employed for MALDI-MSI experiments. The list of identified proteins and their peptides is provided in the supplementary material (**supplementary material table 1 and 2**). Their functional analysis was performed using STRING 8.3 (**figure 7**) to observe and visualize correlations between the identified proteins and their role. The resulting STRING protein interaction map showed clearly that many proteins that we have identified and localized are connected. The figure shows two principal groups of proteins that can interact. The first one is the family of collagens that can interact with laminin subunit alpha (LAMA5), and proteins from the desintegrin family like ATS2 or ADMAST2, interleukin 18 (IL-18) and death domain-associated protein 6 (DAXX). These proteins are known for regulating cell survival/death signals, the remodeling of different tissues as well as inflammatory cascades. An influential role of IL 18 in the induction and perpetuation of chronic inflammation has been reported from experimental and clinical rheumatoid synovitis [37]. Recently soluble interleukin-18 receptor complex has been reported as a novel biomarker in rheumatoid arthritis [38]. The second group of proteins comprehend examples like myosin 1 (MYH1), the family of actin proteins and troponin 3 (TNNT3), all of them reported previously as RA markers as indicator of tissue rearrangement. CCAAT/enhancer-binding protein beta (CEBPB) and nuclear receptor coactivator 1 (NCOA1) are indirectly regulating the expression with different proteins of the family of actins. NOCA1 directly binds and interacts with transcription factors such as STAT3 (signal transducer and activator of transcription 3) following IL-6 stimulation and stimulates the transcriptional activities under inflammatory stress [39]. Proteins with similar localization found by MALDI-MSI like TNNT3, collagens and myosin are abundant in muscles and the pathway shows their interaction.

4. Discussion

Mass spectrometry imaging (MSI) is a method with a high potential because it allows the molecular analysis of a tissue while retaining the information about the spatial distribution of different analytes like proteins, peptides, lipids or small molecules. In the last years MSI has been applied for the study of the distribution of

biomarkers, targets of treatment and to classify different stages of a disease. Brain, heart, kidney or breast tissues have been extensively and previously studied by MSI [40-44].

Although it is becoming a technique used for many biological applications a multimodal imaging approach has not been reported before in musculoskeletal tissues. Only some studies have been performed in hard tissues like bone describing the mineral composition [45, 46]. However the most part of these studies have been performed in soft tissues. The importance of the analyses of such complex and heterogeneous tissues is necessary for future studies in diseases that affect different tissues at the same time.

We have chosen a mouse model of RA to explore the limits of TOF-SIMS and MALDI-MSI in tissues that can be affected this pathology. RA is one of the most prevalent rheumatic diseases without an efficient therapy. Here, for the first time, we present the application of MSI to study the distribution of electrolytes, lipids and peptides in the limb of a RA mouse model. The relatively small size of the mouse limb allowed us to perform molecular histology on the entire section surface. Different tissue types such as bone, muscle and skin from both upper and lower limb regions can be appreciated by classical staining techniques. In our workflow distinct classes of various molecules were imaged in a label free manner. For example, we have observed by TOF-SIMS a predominant distribution of potassium in the muscles. In any healthy tissue a balance between potassium and sodium is necessary to preserve the cell homeostasis and integrity. Both ions are involved in ATP generation and muscles contractility. In some rheumatic diseases an imbalance of potassium has been described as dystrophy diseases [47]. Potassium is exceptionally important for formation of the membrane potential and increase in its extracellular concentration can be indicative/causative of biological damage. This element is also what controls the creation as well as the storage of the muscles main source of fuel, glycogen. We have also observed the signal from sodium, highly abundant in bones similar to previous studies [48]. Other electrolytes like calcium were found in muscles and in the femur. Calcium signaling is related to many cellular channels and in the ATP generation and alteration in the calcium pumps have been related to the initiation of adjuvant arthritis [49]. In addition we have found a co-localization of cholesterol and calcium in the muscles. In fact an imbalance in calcium regulation due to cholesterol

abnormal deposition causes endhotelial dysfunction and muscle defects in myocardial diseases [50].

We have also localized different lipids like the PC (head group) with a homogeneous distribution in the entire sample, even in the core of the joint. Many authors have detected PC related species in many tissues using MSI [51, 52]. Other lipids like DAG (m/z 577) is represented in the skin but also in the joint. We have detected deposition of DAG in the upper part of the limb. Other authors showed that signal intensities of fatty acids (FAs) and diacylglycerols (DAGs) were significantly increased in skeletal muscle of the obese ob/ob mice as compared to the lean wild-type mice [53]. DAG and other phospholipids (PL) are responsible for many of the unique physicochemical, biochemical, and biological properties of the cellular membranes. It was suggested that phospholipids present in the synovial fluid (SF) and on the surface of articular cartilage have major involvement in the low friction of cartilage, which is essential for proper mobility of synovial joints. In pathologies, such as impaired biolubrication, there is an imbalance in the levels of phospholipids in the SF [54-56].

By MALDI-MSI we have plotted the distribution of other members of the family of PC. Other authors have shown that a specific pattern of distribution of PC can be studied by MALDI-MSI [57]. For instance, we have found PC 34:1(16:0/18:1) homogeneously distributed. This molecule has been found in high contraction in ischemic rats. This was suggested to be a result of edema and influx of extracellular fluid likely through a loss of Na/K-ATPase caused by the injury. Intact phosphocholines accumulates over the most damaged areas of the dystrophic muscles, together with cholesterol and sphingomyelin species. Fatty acyl chain composition varies depending on the region, allowing estimation of the local damage extension [58]. Tissue digestion and in solution we have identified a high number of proteins. In addition, among the proteins that we have identified a high number of them are regulators of metabolic lipid pathways like choline/ethanolamine kinase (CHKB), glycerophosphocholine phosphodiesterase (GPCP1), diacylglycerol kinase 1beta (DGKQ) choline transporter like protein 1 (CTL1) or inositol1,4,5-triphosphate receptor type 2 (ITPR2). A further analysis in the role of each of these proteins in relation with the different lipid distributions observed in this study are imperative for the proper understanding of the tissue biology.

We have plotted the distribution of some selected identified tryptic peptidesd proteins such as the actin tryptic peptide at *m/z* 1198.7 and myosin tryptic peptide at *m/z* 1885.7, both of them localized in the muscles. The underpinning proteins have been reported as RA markers and as we show in the pathway they are in contact with other proteins identified [25, 59, 60]. Peptides from TBCC, TNN3, COJA1, CO1A2 and PTN12 were also found in the muscles but with a higher concentration in the lower part of the limb. It is interesting the fact that as STRING analysis shows TNNT3 can interact indirectly with the family of collagens and all these proteins have been localized in the same areas. A peptide from the LENG8 and EFCB5 had a completely different localization. Both peptides were highly distributed in the skin and in the ligaments from the lower limb. Leukocyte receptors regulate inflammatory cascades and actually interact with many proteins involved in the rheumatoid pathology like IL-18 [61]. ATS16 and IL-16 were highly distributed in muscles, bones, skin and ligaments. ATS2 also named ADAMTS2 was detected mainly in muscles and bones from the upper and lower limbs. ADAMTS proteases have been associated with a number of different diseases and are of high biomedical relevance such as ADAMTS1 which is upregulated in inflammation [62] while ADAMTS2 and ADAMTS3 are responsible for processing several types of procollagen proteins [63, 64]. Finally, we have demonstrated the capability that ion mobility separation offers allowing us the visualization of molecules that otherwise couldn’t be seen.

5. Conclusions

We have demonstrated that a multimodal MSI workflow combined with classical bottom up proteomic approach is an efficient tool for detection and localization of a variety of molecules directly from musculoskeletal tissue sections. The application of this method in future studies could be helpful to understand the changes of the molecular distribution in tissues that are affected by rheumatic diseases.

Acknowledgments

This work is part of the research program of the "Stichting voor Fundamenteel Onderzoek der Materie (FOM)", which is financially supported by the "Nederlandse organisatie voor Wetenschappelijk Onderzoek (NWO)". Authors also acknowledge

funding through the EC Project for targeted delivery of nanomedicine MEDITRANS (FP VI 2006, EU IP NMP-26668).

Figure captions

Figure 1

Schematic experiment design. RA mouse limbs were cryo-sectioned into 12-µm thin sections for multimodal mass spectrometric imaging. High spatial resolution imaging by SIMS-TOF required tissue coating with gold. For lipid visualization tissue sections were covered with matrix and analyzed by MALDI-TOF. Peptide imaging required on-tissue digestion of proteins, followed by matrix application and MALDI analysis. Orthogonally, a protocol for protein identification was performed.

Figure 2

High spatial resolution SIMS imaging of lipids and smaller ions. The dot line marked region indicates the joint and the attached bone areas. (A) The total ion image of the tissue section. (B-F) The overlay images of three different ions of interest: (B) Potassium (*m/z* 39) in red, sodium (*m/z* 23) in green and indium as overlay background (*m/z* 115) in blue. (C) Phosphocholine (*m/z* 184) in red, PC 36:0 (*m/z* 791) in green and a diacylglycerol (*m/z* 577) in blue. (D) Cholesterol (*m/z* 369) in red, potassium (*m/z* 39) in green and indium as overlay background (*m/z* 115) in blue. (E) Cholesterol (*m/z* 369) in red, a diacylglycerol (*m/z* 577) in green and indium as overlay background (*m/z* 115) in blue. (F) Cholesterol (*m/z* 369) in red, calcium (*m/z* 40) in green and indium as overlay background (*m/z* 115) in blue. Distribution of different types of ions marks the different regions of the tissue section. Scale bars, 1 mm.

Figure 3

Distribution of lipid molecules in the tissue section. Distribution of lipid ions such as (A) PC 32:0(16:0/16:0) $[M+H]^+$ at *m/z* 734.5; (B) PC 34:2(16:0/18:2) $[M+H]^+$ at *m/z* 758.5; (C) PC 34:1(16:0/18:1) $[M+H]^+$ at *m/z* 760.5; (D) PC 36:1(18:0/18:1) $[M+H]^+$ at

m/z 788.5; (E) PC 34:2(16:0/18:2) $[M+K]^+$ at *m/z* 796.5 and (F) PC 40:6(18:0/22:6) $[M+H]^+$ at *m/z* 834.5 detected in upper and/or lower limb regions.

Figure 4

The experimentally determined distribution of various peptides from abundant and less abundant proteins. (A) Distribution of actin tryptic peptide at *m/z* 1198.7. (B) Distribution of myosin tryptic peptide at *m/z* 1855.8. (C) Distribution of tubulin tryptic peptide at *m/z* 1960.0. Distribution of peptides obtained from less abundant proteins such as (D) troponin T tryptic peptide at *m/z* 1887.9, (E) collagen alpha-1(XIX) chain at *m/z* 1584.8, (F) collagen alpha-2(I) chain at *m/z* 1561.8, (G) tyrosine-protein phosphatase non-receptor type 12 at *m/z* 1654.8, (H) leukocyte receptor cluster member 8 homolog at *m/z* 1027.8 and (I) EF-hand calcium-binding domain-containing protein 5 at *m/z* 1197.7.

Figure 5

The experimentally determined distribution of various peptides from proteins related to RA. (A) Distribution of the disintegrin and metalloproteinase with thrombospondin motifs 16 protein tryptic peptide at *m/z* 1347.7. (B) Distribution of the pro-interleukin-16 tryptic peptide at *m/z* 1404.7. (C) Distribution of the disintegrin and metalloproteinase with thrombospondin motifs 2 tryptic peptide at *m/z* 1838.9.

Figure 6

Ion mobility analysis of biomolecules detected from the tissue sections. (A) Spectrum of detected ions in the mass range *m/z* 650-950. (B) Drift time versus *m/z* plot showing ion mobility separated lipid and matrix ions (encircled). (C) Distribution of the ion mobility separated background ion at *m/z* 721.41. (D) Distribution of the ion mobility separated ion at *m/z* 721.49.

Figure 7

STRING protein-protein interaction map showing interactions of proteins detected from the section of the RA mouse model. A number of interesting proteins like disintegrin and metalloproteinase family (ADAMTS2), collagens (COL), actins (ACT), myosins (MYH), troponin (TNNT3) and interleukin 18 (IL18) interacted in pathways related to RA. Some of these proteins were identified and localized.

Supplementary figure 1

Multimodal imaging of a limb in a RA mouse. (A) Optical image of the tissue marked with different regions (B) H&E stained 12-µm section. (C) SIMS high spatial resolution total ion image. (D) MALDI ion image at *m/z* 760.5.

References

1. Chughtai, K. and R.M. Heeren, *Mass spectrometric imaging for biomedical tissue analysis.* Chem. Rev., 2010. **110**(5): p. 3237-77.
2. Skold, K., et al., *Decreased striatal levels of PEP-19 following MPTP lesion in the mouse.* J Proteome Res, 2006. **5**(2): p. 262-9.
3. Rohner, T.C., D. Staab, and M. Stoeckli, *MALDI mass spectrometric imaging of biological tissue sections.* Mech Ageing Dev, 2005. **126**(1): p. 177-85.
4. Roy, S., et al., *Imaging mass spectrometry: a new tool for the analysis of skin biopsy. Application in Fabry's disease.* Ann. Pharm. Fr., 2006. **64**(5): p. 328-34.
5. Debois, D., et al., *In situ lipidomic analysis of nonalcoholic fatty liver by cluster TOF-SIMS imaging.* Anal. Chem., 2009. **81**(8): p. 2823-31.
6. Touboul, D., et al., *Changes of phospholipid composition within the dystrophic muscle by matrix-assisted laser desorption/ionization mass spectrometry and mass spectrometry imaging.* Eur. J. Mass Spectrom., 2004. **10**(5): p. 657-64.
7. Herring, K.D., S.R. Oppenheimer, and R.M. Caprioli, *Direct tissue analysis by matrix-assisted laser desorption ionization mass spectrometry: application to kidney biology.* Semin. Nephrol., 2007. **27**(6): p. 597-608.
8. Djidja, M.C., et al., *MALDI-ion mobility separation-mass spectrometry imaging of glucose-regulated protein 78 kDa (Grp78) in human formalin-fixed, paraffin-embedded pancreatic adenocarcinoma tissue sections.* J. Proteome Res., 2009. **8**(10): p. 4876-84.
9. Schwamborn, K., et al., *Identifying prostate carcinoma by MALDI-Imaging.* Int. J. Mol. Med., 2007. **20**(2): p. 155-9.
10. Lemaire, R., et al., *Specific MALDI imaging and profiling for biomarker hunting and validation: fragment of the 11S proteasome activator complex, Reg alpha fragment, is a new potential ovary cancer biomarker.* J. Proteome Res., 2007. **6**(11): p. 4127-34.
11. Yanagisawa, K., et al., *Proteomic patterns of tumour subsets in non-small-cell lung cancer.* Lancet, 2003. **362**(9382): p. 433-9.
12. Shimma, S., et al., *MALDI-based imaging mass spectrometry revealed abnormal distribution of phospholipids in colon cancer liver metastasis.* J. Chromatogr., B: Anal. Technol. Biomed. Life Sci., 2007. **855**(1): p. 98-103.
13. Scott, D.L., F. Wolfe, and T.W. Huizinga, *Rheumatoid arthritis.* Lancet, 2010. **376**(9746): p. 1094-108.
14. Kantor, A.B., et al., *Biomarker discovery by comprehensive phenotyping for autoimmune diseases.* Clin Immunol, 2004. **111**(2): p. 186-95.

15. Ali, M. and N. Manolios, *Proteomics in rheumatology: a new direction for old diseases.* Semin Arthritis Rheum, 2005. **35**(2): p. 67-76.
16. Li, T.W., et al., *Screening disease-associated proteins from sera of patients with rheumatoid arthritis: a comparative proteomic study.* Chin Med J (Engl), 2010. **123**(5): p. 537-43.
17. Sinz, A., et al., *Mass spectrometric proteome analyses of synovial fluids and plasmas from patients suffering from rheumatoid arthritis and comparison to reactive arthritis or osteoarthritis.* Electrophoresis, 2002. **23**(19): p. 3445-56.
18. Liao, H., et al., *Use of mass spectrometry to identify protein biomarkers of disease severity in the synovial fluid and serum of patients with rheumatoid arthritis.* Arthritis Rheum, 2004. **50**(12): p. 3792-803.
19. Blaser, J., et al., *Determination of metalloproteinases, plasminogen-activators and their inhibitors in the synovial fluids of patients with rheumatoid arthritis during chemical synoviorthesis.* Clin Chim Acta, 1996. **244**(1): p. 17-33.
20. Jones, H.W., et al., *Inactivation of antithrombin III in synovial fluid from patients with rheumatoid arthritis.* Ann Rheum Dis, 1998. **57**(3): p. 162-5.
21. Bresnihan, B., et al., *Apolipoprotein A-I infiltration in rheumatoid arthritis synovial tissue: a control mechanism of cytokine production?* Arthritis Res Ther, 2004. **6**(6): p. R563-R566.
22. Gonzalez-Gronow, M., G. Gawdi, and S.V. Pizzo, *Characterization of the plasminogen receptors of normal and rheumatoid arthritis human synovial fibroblasts.* J Biol Chem, 1994. **269**(6): p. 4360-6.
23. Misra, U.K., et al., *Up-regulation of the alpha2-macroglobulin signaling receptor on rheumatoid synovial fibroblasts.* J Biol Chem, 1997. **272**(1): p. 497-502.
24. Schedel, J., et al., *Differential adherence of osteoarthritis and rheumatoid arthritis synovial fibroblasts to cartilage and bone matrix proteins and its implication for osteoarthritis pathogenesis.* Scand J Immunol, 2004. **60**(5): p. 514-23.
25. Zheng, X., et al., *Study of the human plasma proteome of rheumatoid arthritis.* J Chromatogr A, 2009. **1216**(16): p. 3538-45.
26. Doherty, N.S., et al., *Analysis of changes in acute-phase plasma proteins in an acute inflammatory response and in rheumatoid arthritis using two-dimensional gel electrophoresis.* Electrophoresis, 1998. **19**(2): p. 355-63.
27. Ukaji, F., et al., *Serum samples of patients with rheumatoid arthritis contain a specific autoantibody to "denatured" aldolase A in the osteoblast-like cell line, MG-63.* Ann Rheum Dis, 1999. **58**(3): p. 169-74.
28. Tchetverikov, I., et al., *Active MMPs captured by alpha 2 macroglobulin as a marker of disease activity in rheumatoid arthritis.* Clin Exp Rheumatol, 2003. **21**(6): p. 711-8.
29. Giusti, L., et al., *Is GRP78/BiP a potential salivary biomarker in patients with rheumatoid arthritis?* Proteomics Clin Appl, 2010. **4**(3): p. 315-24.
30. Justen, H.P., et al., *Differential gene expression in synovium of rheumatoid arthritis and osteoarthritis.* Mol Cell Biol Res Commun, 2000. **3**(3): p. 165-72.
31. Hsu, H.C., et al., *Production of a novel class of polyreactive pathogenic autoantibodies in BXD2 mice causes glomerulonephritis and arthritis.* Arthritis Rheum, 2006. **54**(1): p. 343-55.
32. Ananth, L., P.E. Prete, and M.L. Kashyap, *Apolipoproteins A-I and B and cholesterol in synovial fluid of patients with rheumatoid arthritis.* Metabolism, 1993. **42**(7): p. 803-6.
33. Brand, D.D., K.A. Latham, and E.F. Rosloniec, *Collagen-induced arthritis.* Nat Protoc, 2007. **2**(5): p. 1269-75.

34. Tang, B., et al., *Pathogenesis of collagen-induced arthritis: modulation of disease by arthritogenic T-cell epitope location.* Immunology, 2004. **113**(3): p. 384-91.
35. Brand, D.D., A.H. Kang, and E.F. Rosloniec, *The mouse model of collagen-induced arthritis.* Methods Mol Med, 2004. **102**: p. 295-312.
36. Kiss, A. and R.M. Heeren, *Size, weight and position: ion mobility spectrometry and imaging MS combined.* Anal Bioanal Chem, 2011. **399**(8): p. 2623-34.
37. Liew, F.Y., X.Q. Wei, and I.B. McInnes, *Role of interleukin 18 in rheumatoid arthritis.* Ann Rheum Dis, 2003. **62 Suppl 2**: p. ii48-50.
38. Takei, S., et al., *Soluble interleukin-18 receptor complex is a novel biomarker in rheumatoid arthritis.* Arthritis Res Ther. **13**(2): p. R52.
39. Giraud, S., et al., *Functional interaction of STAT3 transcription factor with the coactivator NcoA/SRC1a.* J Biol Chem, 2002. **277**(10): p. 8004-11.
40. Kim, C.W., et al., *Determination of spatial distribution of melamine-cyanuric acid crystals in rat kidney tissue by histology and imaging matrix-assisted laser desorption/ionization quadrupole time-of-flight mass spectrometry.* Chem Res Toxicol, 2010. **23**(1): p. 220-7.
41. Altelaar, A.F., et al., *Gold-enhanced biomolecular surface imaging of cells and tissue by SIMS and MALDI mass spectrometry.* Anal Chem, 2006. **78**(3): p. 734-42.
42. Grey, A.C., et al., *Molecular morphology of the chick heart visualized by MALDI imaging mass spectrometry.* Anat Rec (Hoboken), 2010. **293**(5): p. 821-8.
43. Manicke, N.E., et al., *Imaging of lipids in atheroma by desorption electrospray ionization mass spectrometry.* Anal Chem, 2009. **81**(21): p. 8702-7.
44. Kaneko, Y., et al., *Imaging mass spectrometry analysis reveals an altered lipid distribution pattern in the tubular areas of hyper-IgA murine kidneys.* Exp Mol Pathol, 2011. **91**(2): p. 614-21.
45. Eriksson, C., P. Malmberg, and H. Nygren, *Time-of-flight secondary ion mass spectrometric analysis of the interface between bone and titanium implants.* Rapid Commun Mass Spectrom, 2008. **22**(7): p. 943-9.
46. Malmberg, P. and H. Nygren, *Methods for the analysis of the composition of bone tissue, with a focus on imaging mass spectrometry (TOF-SIMS).* Proteomics, 2008. **8**(18): p. 3755-62.
47. McDonough, A.A., C.B. Thompson, and J.H. Youn, *Skeletal muscle regulates extracellular potassium.* Am J Physiol Renal Physiol, 2002. **282**(6): p. F967-74.
48. Bushinsky, D.A., et al., *Contribution of organic material to the ion composition of bone.* J Bone Miner Res, 2000. **15**(10): p. 2026-32.
49. Strosova, M.K., et al., *Modulation of sarcoplasmic/endoplasmic reticulum Ca(2+)-ATPase activity and oxidative modification during the development of adjuvant arthritis.* Arch Biochem Biophys, 2011. **511**(1-2): p. 40-7.
50. Saini, H.K., A.S. Arneja, and N.S. Dhalla, *Role of cholesterol in cardiovascular dysfunction.* Can J Cardiol, 2004. **20**(3): p. 333-46.
51. Nygren, H., et al., *Localization of cholesterol, phosphocholine and galactosylceramide in rat cerebellar cortex with imaging TOF-SIMS equipped with a bismuth cluster ion source.* Biochim Biophys Acta, 2005. **1737**(2-3): p. 102-10.
52. Amstalden van Hove, E.R., et al., *Multimodal mass spectrometric imaging of small molecules reveals distinct spatio-molecular signatures in differentially metastatic breast tumor models.* Cancer Res, 2010. **70**(22): p. 9012-21.
53. Magnusson, Y.K., et al., *TOF-SIMS analysis of lipid accumulation in the skeletal muscle of ob/ob mice.* Obesity (Silver Spring), 2008. **16**(12): p. 2745-53.
54. Agren, J.J., et al., *Divergent changes in serum sterols during a strict uncooked vegan diet in patients with rheumatoid arthritis.* Br J Nutr, 2001. **85**(2): p. 137-9.

55. Angel, J., et al., *Interleukin-1-mediated phospholipid breakdown and arachidonic acid release in human synovial cells.* Arthritis Rheum, 1993. **36**(2): p. 158-67.
56. Bomalaski, J.S. and M.A. Clark, *Phospholipase A2 and arthritis.* Arthritis Rheum, 1993. **36**(2): p. 190-8.
57. Hankin, J.A., et al., *MALDI mass spectrometric imaging of lipids in rat brain injury models.* J Am Soc Mass Spectrom, 2011. **22**(6): p. 1014-21.
58. Tahallah, N., et al., *Lipid mapping in human dystrophic muscle by cluster-time-of-flight secondary ion mass spectrometry imaging.* J Lipid Res, 2008. **49**(2): p. 438-54.
59. McDonald, B.L., R.L. Dawkins, and J. Robinson, *Myosin autoantibodies reacting with selective muscle fiber types.* Muscle Nerve, 1979. **2**(1): p. 37-43.
60. Shrivastav, M., et al., *Autoantibodies against cytoskeletal proteins in rheumatoid arthritis.* Clin Rheumatol, 2002. **21**(6): p. 505-10.
61. Volin, M.V. and A.E. Koch, *Interleukin-18: a mediator of inflammation and angiogenesis in rheumatoid arthritis.* J Interferon Cytokine Res, 2011. **31**(10): p. 745-51.
62. Kuno, K., et al., *Molecular cloning of a gene encoding a new type of metalloproteinase-disintegrin family protein with thrombospondin motifs as an inflammation associated gene.* J Biol Chem, 1997. **272**(1): p. 556-62.
63. Colige, A., et al., *cDNA cloning and expression of bovine procollagen I N-proteinase: a new member of the superfamily of zinc-metalloproteinases with binding sites for cells and other matrix components.* Proc Natl Acad Sci U S A, 1997. **94**(6): p. 2374-9.
64. Hurskainen, T.L., et al., *ADAM-TS5, ADAM-TS6, and ADAM-TS7, novel members of a new family of zinc metalloproteases. General features and genomic distribution of the ADAM-TS family.* J Biol Chem, 1999. **274**(36): p. 25555-63.

Figure 1

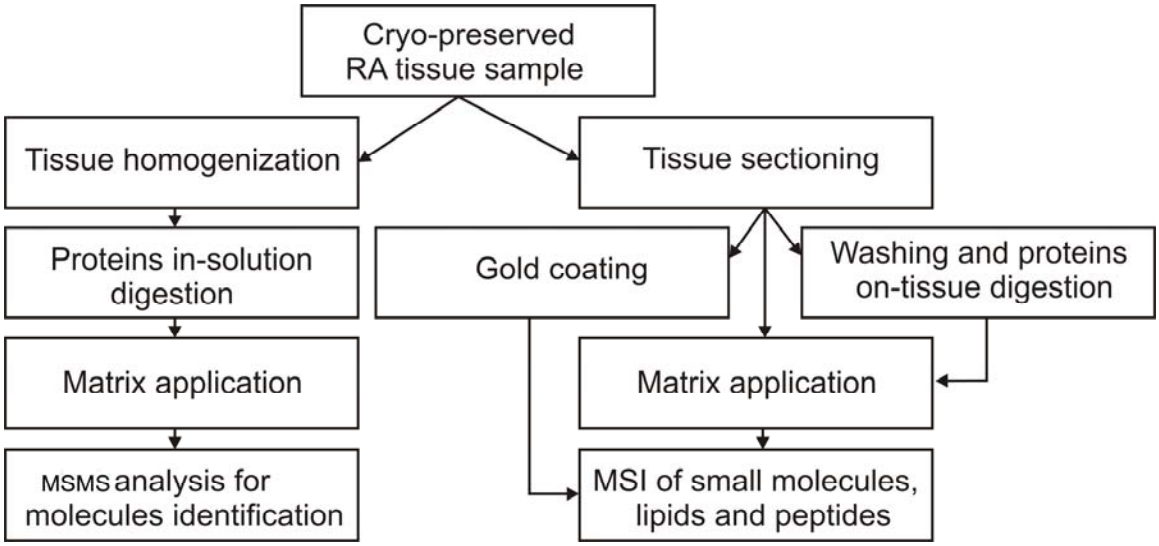
Cryo-preserved
RA tissue sample
Tissue homogenization
Tissue sectioning
Proteins in-solution
digestion
Gold coating
Washing and proteins
on-tissue digestion
Matrix application
Matrix application
MSMS analysis for
molecules identification
MSI of small molecules,
lipids and peptides

Figure 2

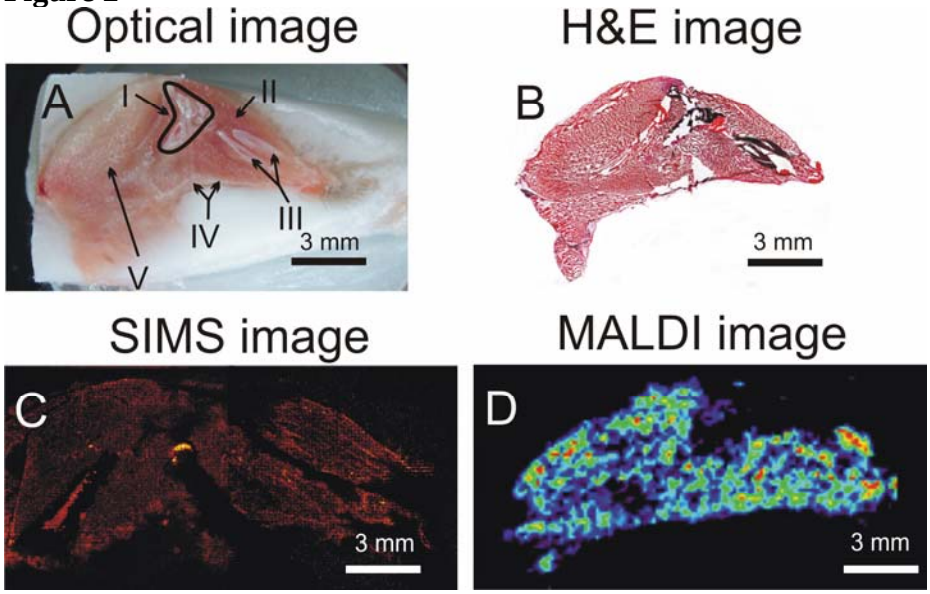
Optical image
H&E image
A
I
II
III
IV
V
3 mm
B
3 mm
SIMS image
MALDI image
C
3 mm
D
3 mm

Figure 3

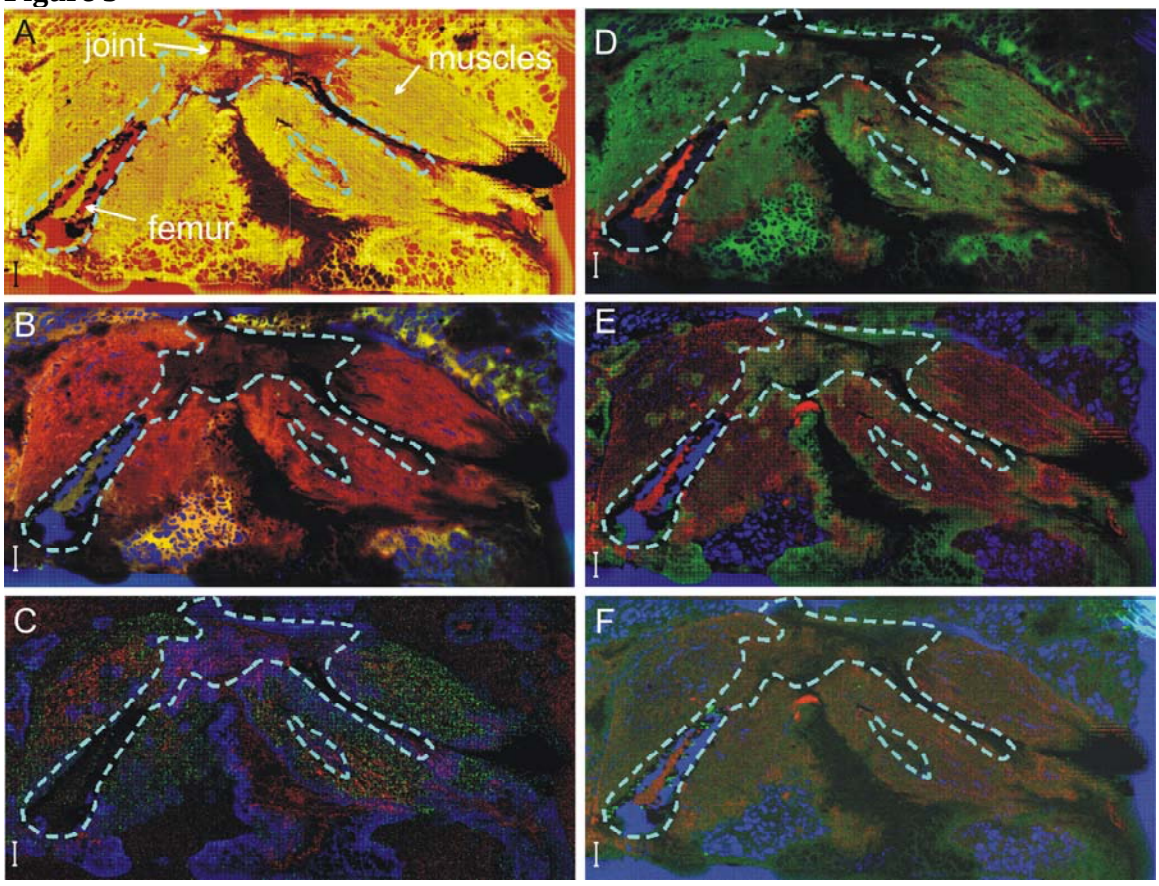

Figure 4

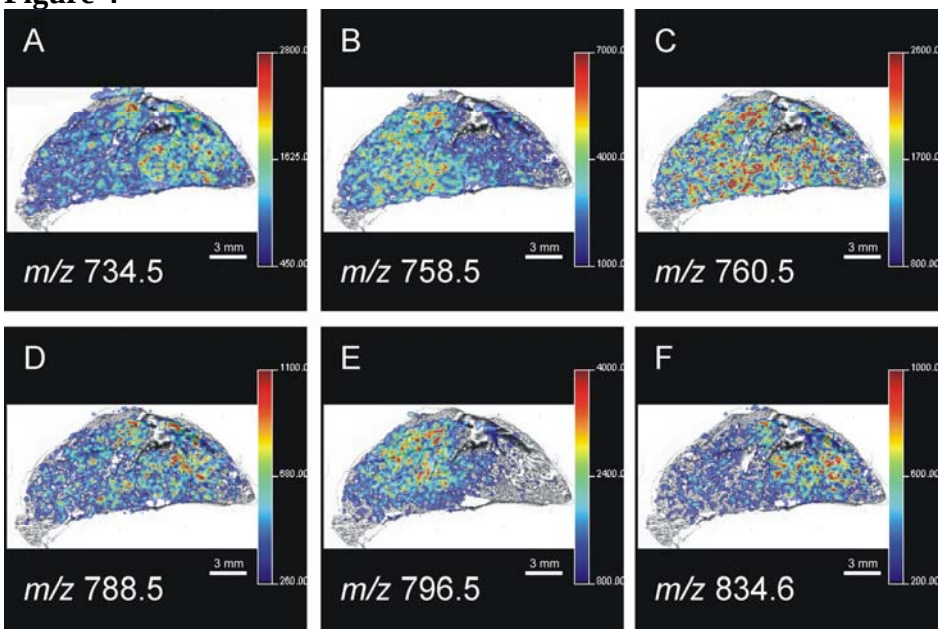
A
m/z 734.5
3 mm
B
m/z 758.5
3 mm
C
m/z 760.5
3 mm
D
m/z 788.5
3 mm
E
m/z 796.5
3 mm
F
m/z 834.6
3 mm

Figure 5

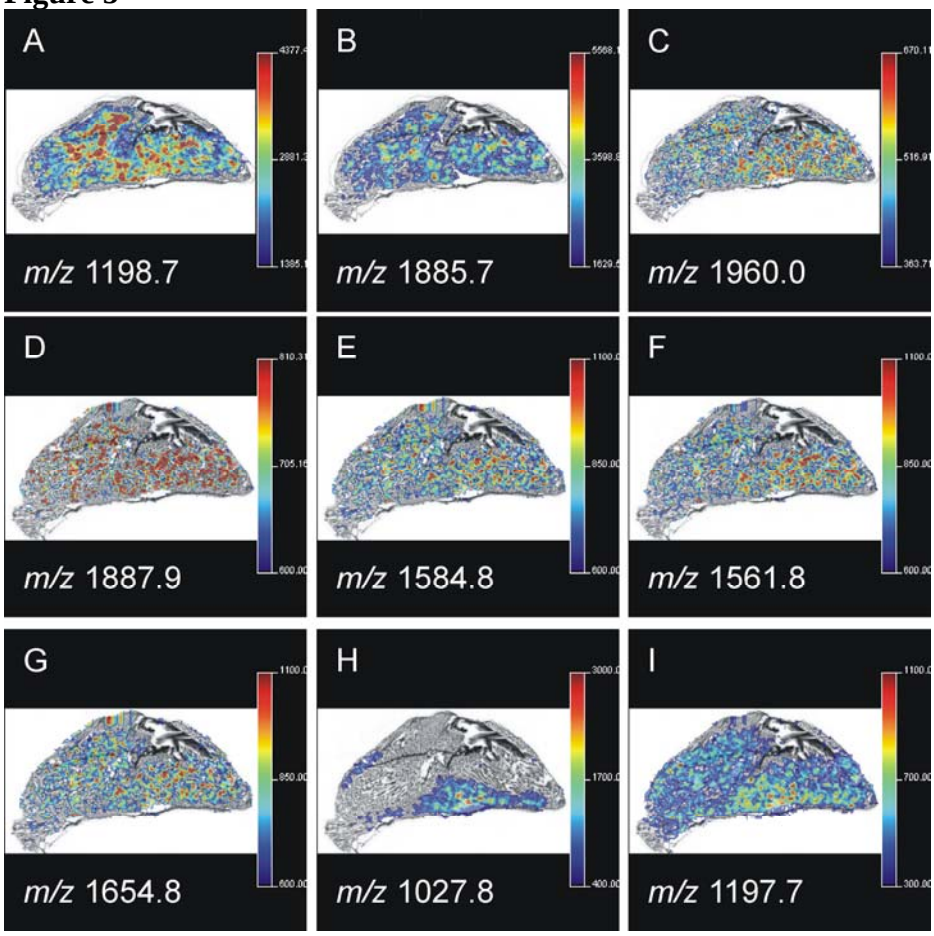
A
m/z 1198.7
B
m/z 1885.7
C
m/z 1960.0
D
m/z 1887.9
E
m/z 1584.8
F
m/z 1561.8
G
m/z 1654.8
H
m/z 1027.8
I
m/z 1197.7

Figure 6

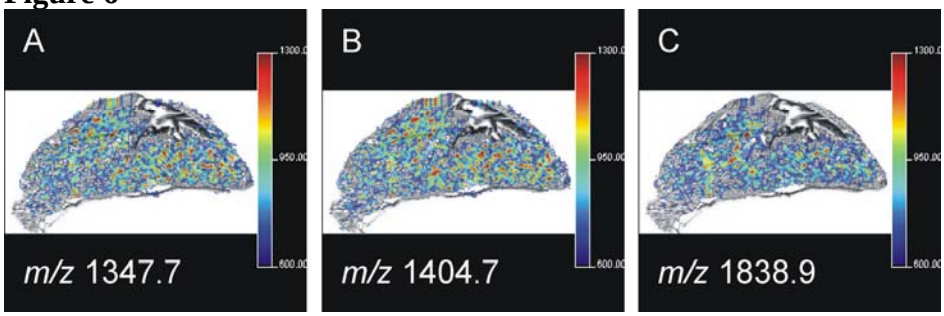
A
1300.0
950.00
600.00
m/z 1347.7
B
1300.0
950.00
600.00
m/z 1404.7
C
1300.0
950.00
600.00
m/z 1838.9

Figure 7

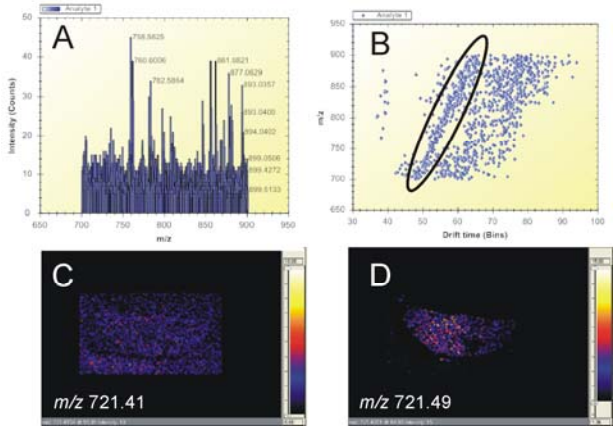

Figure 8

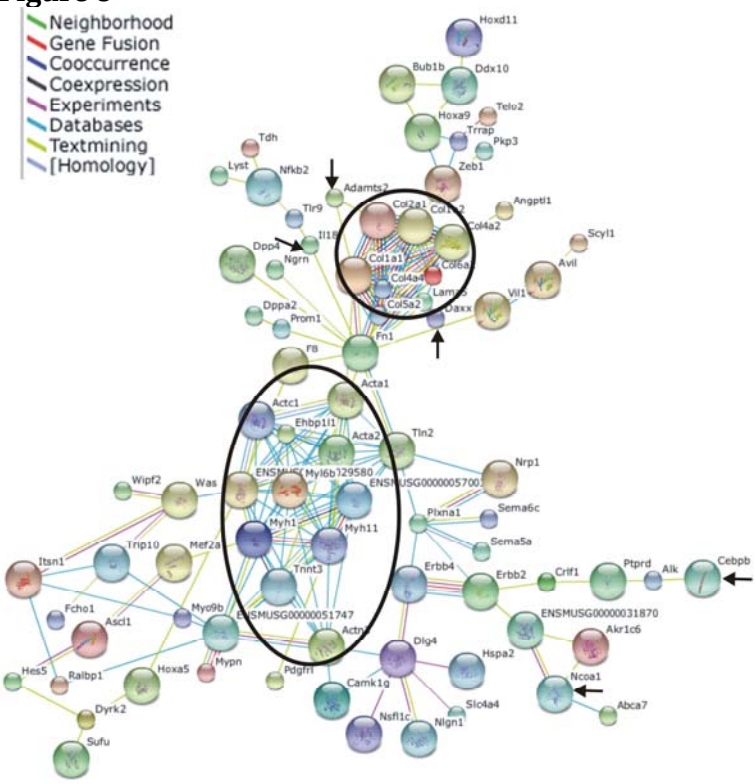
Neighborhood
Gene Fusion
Cooccurrence
Coexpression
Experiments
Databases
Textmining
[Homology]
Hoxd11
Bub1b
Ddx10
Telo2
Hoxa9
Trrap
Pkp3
Tdh
Lyst
Nfkb2
Zeb1
Adamts2
Tlr9
Col2a1
Angptl1
Col4a2
Il1b
Scyl1
Dpp4
Ngrn
Col1a1
Col5a1
Avil
Col4a1
Lamb3
Vil1
Col5a2
Daxx
Dppa2
Prom1
Fn1
F8
Acta1
Actc1
Ehbp1l1
Acta2
Tln2
Nrp1
Wipf2
Was
ENSMUSG00000057001
Myl6b
129580
Sema6c
Plxna1
Myh1
Myh11
Sema5a
Trip10
Mef2a
Itsn1
Tnnt3
Erbb4
Crif1
Ptprd
Alk
Cebpb
Erbb2
Fcho1
Ascl1
Myo9b
ENSMUSG00000051747
Actn1
ENSMUSG00000031870
Akr1c6
Dlg4
Hspa2
Hes5
Ralbp1
Hoxa5
Mypn
Pdgfrl
Camk1g
Ncoa1
Dyrk2
Slc4a4
Abca7
Nsfl1c
Nlgn1
Sufu